

Experimental and CFD modelling of indoor air and wake flow from a moving manikin

Yao Tao¹, Kiao Inthavong¹, Phred Petersen², Krishna Mohanarangam³, William Yang³, Jiyuan Tu¹

¹ School of Engineering, RMIT University, Bundoora, Australia

² School of Media and Communications, RMIT University, Melbourne, Australia

³ CSIRO Mineral Resources, Clayton, Australia

Abstract

The effect of human motion on wake flow dynamics and particle dispersion were investigated by experimental visualisation and Computational Fluid Dynamics (CFD) modelling using a mannequin model with realistic human shape. A new smoke visualisation technique is proposed which made use of the chemical reaction between acetic acid and cyclohexylamine. The CFD model used a dynamic mesh to simulate the moving manikin, and the Lagrangian particle tracking for particle dispersion originating from the floor. The results showed the moving manikin sheared the stagnant air and entrained flow, inducing a wake that gathered momentum as the manikin moved forwards. Using the smoke visualisation technique, we were able to visualise the trailing smoke passing over the manikin which had come to a stop. The passing wake enhanced inhalation exposure as it has potential to re-disperse particles into the breathing region.

Introduction

Human induced wake flow yields significant influence on particle dispersion and resuspension affecting exposure levels and particulate matter (PM) sampling readings. Recent computational studies of airflow around the human body have revealed its influence in transporting particles into the breathing region, promoting inhaled particle exposure [1-4]. However, these studies used a stationary human model/manikin under exposure. Computational modelling of moving human/manikins through indoor spaces observed vortices in the wake region which causes significant dispersion of contaminants in the surrounding environment [5-7]. Other CFD models using a coupled Lagrangian and Immersed Boundary Method found that a faster human walking speed could effectively reduce the transport or suspension of contaminants within a room [8] or between room compartments [9].

Experimental studies have confirmed the occurrence of particle resuspension caused by human activities. [10] used optical particle counters in a full scale test chamber and showed that 'heavy and fast' walking produced higher resuspension rates than less active walking. This was attributed to a combination of increased pace, increased air swirl velocity, and electrostatic field effects established by the walking. Similarly studies investigated human interactions with floor type [11], dust type and contaminant concentration in dust loads [12]. These studies provide direct cause and effect relationships between human activity, environment, and dust resuspension. However, its use for verifying CFD simulation data of moving human subjects/manikins is difficult.

Experimental studies of human induced wake flows are one way to validate CFD models. It also provides insight into the fluid dynamics mechanisms that transport the particles during resuspension. Early experimental studies of human induced wake

flows [13,14] used a manikin installed in an open-ended wind tunnel, and tracer gases were released from different locations to visualise boundary layer separation, and the size and location of the wake region. To date no experimental work has been performed to reproduce the wake flow induced by a walking human. This is partly due to the challenges in flow visualisation techniques to capture a dynamic flow field rather than traditional steady state flows. Smoke visualisation is an alternative approach that is most suitable for obtaining qualitative understanding of the gross flow field. Recent studies have demonstrated the ability to capture separation points, reattachment points, and vortex shedding phenomena [15,16]. Traditional smoke visualisation methods involve an alkane chemical such as mineral oil evaporating off a heated smoke-wire and allowed to streak through moving air in a wind tunnel. However, this would not work well for a moving manikin in a still environment due to complexity in setup and operation.

In this study we present an experimental and CFD study of a wake flow induced by a moving human manikin. We present a new technique that allows visualisation of the wake development during the manikin motion and its after effects when the manikin comes to a stop - a key component of particle resuspension. Smoke was produced through a chemical reaction between a saturated chamber of acetic acid and a manikin dabbed with cyclohexylamine. High speed photography captured the transient wake flow development and the image processing was used to produce quantitative data. CFD simulations were performed to visualise fluid and particle flow dynamics, and its effect on particle resuspension.

Materials/Methods

Experimental Setup

A 1/5th scaled indoor room was created from perspex with dimensions of 1100 mm x 600 mm x 800 mm (Fig 1a). Two containers of acetic acid were placed on the floor and allowed to evaporate into the air. A CPU-fan was used to increase the evaporation rate and obtain a well-mixed room condition. An exhaust vent was connected to the ceiling to purge the chamber after each experimental run. A manikin (340mm height) was 3D-printed at RMIT University's Advanced Manufacturing Precinct (Melbourne, Australia) and fixed onto a rack-and-pinion motorised travelator that moved the manikin across length of the test chamber. Small circular felt material (approximately 1cm-diameter) were stuck on the manikin in different locations and cyclohexylamine was dabbed onto its surface. Smoke was generated via a chemical reaction between acetic acid (CH₃COOH) and cyclohexylamine (C₆H₁₃N). The reaction produced smoke (comprised of suspended opaque amine salt particles) suitable for flow visualisation with a high speed camera. A black background was used to provide strong contrast when light scattering illuminated the smoke.

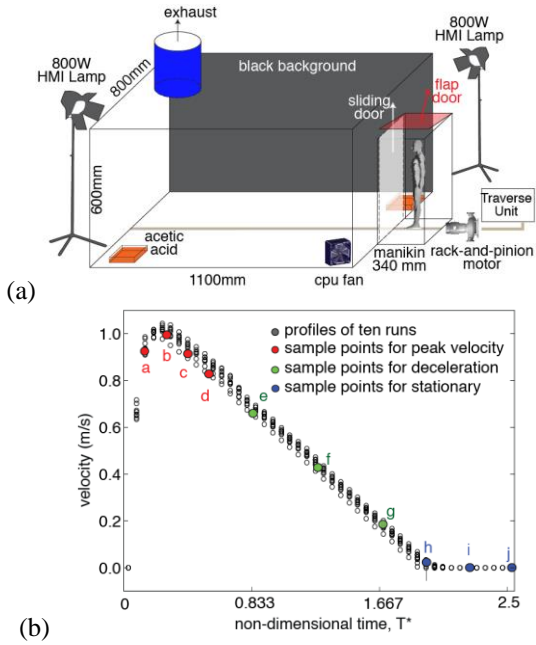


Figure 1. (a) experimental setup schematic (b) manikin velocity profile

The manikin accelerated from rest inside the holding chamber to a peak velocity of $u_{peak} = 1\text{m/s}$ before coming to a complete stop after distance, $s = 0.6\text{m}$ with velocity profile shown in Fig 1b. We use a non-dimensional time T^* defined as $T^* = t \times u_{peak}/S$ where t is the real experimental run time in seconds. A Phantom Miro M310 high speed camera with a Canon 90mm f/2.8 shift lens was used to capture the trailing smoke from the manikin. Two 800W Broncolor HMI (Hydrargyrum Medium-Arc Iodine) lamps with PAR (parabolic aluminized reflector) reflectors and MFL-UV filter glasses were placed behind and to each side of the perspex test chamber, providing sufficient light scattering and illumination of the smoke.

CFD Flow Model Setup

The computational domain was a full 1:1 scale model with dimensions of 4.0m (x -coordinate) \times 6.5m (y -coordinate) \times 3.0m (z -coordinate). The manikin (1.7m -height, 0.58m -width) was centred at $x=0\text{m}$, and inside the y -coordinate by 1m ($y=1\text{m}$), shown in Fig 2(a). The manikin moved with a $1/5^{\text{th}}$ scaled velocity profile to maintain the same Reynolds number matching with the experiment tests. The manikin surface was filled with unstructured tetrahedral cells and 10 prism layer cells with a grid spacing of $1 \times 10^{-4}\text{m}$ (for boundary layer separation), while the external room contained structured hexahedral cells (Fig 2(b) and (c)).

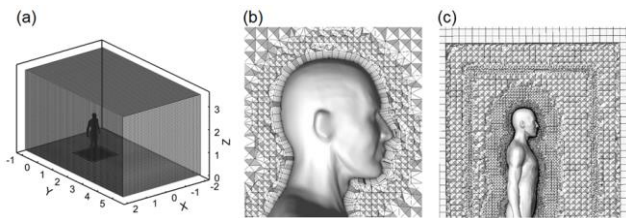


Figure 2 (a) Computational domain of room, x- y- z- coordinates are in metres; (b) Prism layers and mesh generation around the manikin surface (c) hex-core cell elements used in the room environment.

A grid independence study was conducted by reducing individual cell spacing by a factor of 1.3 consecutively and plotting the velocity magnitude along a horizontal and vertical line behind the manikin (Figure 3). The horizontal line was 0.25m behind the body at a height of 1.0m (labelled line-1), while the vertical line was centered and 0.25m behind the body (labelled line-2). We

started with a grid of 0.9million and subsequent grids of 1.7million, 3.6million, and 6.9million were made. The velocity profiles showed convergence between mesh size 3.6 million and 6.9 million and for computational efficiency and accuracy, the 3.6 million model was chosen for the remainder of the study.

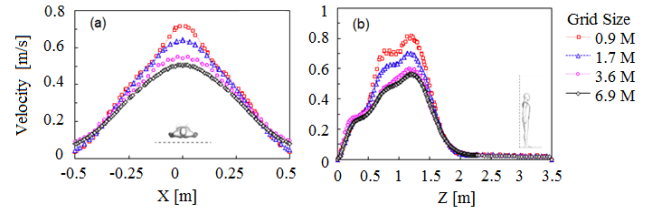


Figure 3 Mesh Independence study: Velocity magnitude at line1 and line2 with respect to different mesh scales.

Because the manikin exhibited an irregular shape, flow separation across different sections of the body can be considered locally. If we consider horizontal separation at the waist (hydraulic diameter $D_h = 0.054\text{m}$, and head ($D_h = 0.037\text{m}$), then the resulting Reynolds number at peak velocity of 1m/s are 2500, and 3600. For separation in the vertical axis we can consider the manikin height ($D_h = 0.34\text{m}$) as its hydraulic diameter which produces $Re = 22,600$; although the separation is not entirely complete from head to toe of the manikin. External flow over cylinders exhibit turbulence for $Re > 20,000$ suggesting that a laminar flow model could be feasible for capturing the flow separation from the moving manikin. Therefore, a transient flow simulation was performed with a time step size of $t = 0.005\text{s}$. The flow was modelled as laminar; but the 3 turbulence models (RNG, SKE and $k\omega$ -SST) were also used to ensure that the model was laminar dominant, and to show the effects of using a fully turbulent model.

Particle Modelling

The Lagrangian particle trajectory-tracking model was used to determine particle transport and re-suspension. Particles of $2.5\mu\text{m}$ were uniformly distributed across the entire floor area of $5.5\text{m} \times 4.0\text{m}$. To test the particle number independence, uniform particle spacings of $(\Delta x, \Delta y)$ 0.05m , 0.02m , 0.01m and 0.005m were evaluated. This corresponded to particle numbers of approximately 8,000, 54,000, 217,000 and 867,000. By plotting the particle concentration on the vertical mid-plane after a walking distance of 2 meters, the amount of particles and its concentration distribution remained almost unchanged for particle number of 217,000 and 867,000, and particle number independence was assumed for 217,000 particles.

Results

Viscous modelling for flow separation across the head

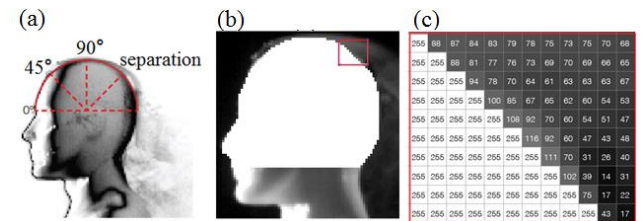


Figure 4 Image processing steps for determining the separation angle point along the head. The pixel values in panel are greyscale values where 255 = white, and 0 = black

The experimental images were processed using threshold segmentation to identify the separation angle across the top of the head. We defined a semi-circle that fitted around the top half of the head, and at eye-level. Fig. 4a shows an example, taken at time $T^*=0.417\text{s}$. The head was partially segmented (using an image mask) out of each image to provide a clear boundary

around the head shown in panel (Fig. 4b). The algorithm then searches along the edge boundary to detect pixel greyscale values. Separation was determined if within three horizontal pixels to an edge pixel (greyscale = 255) there was a greyscale value of less than 80 (Figure 4c). A separation angle was calculated for each image and averaged out over 50-images. The resulting separation angle profile over time is shown in Fig 5.

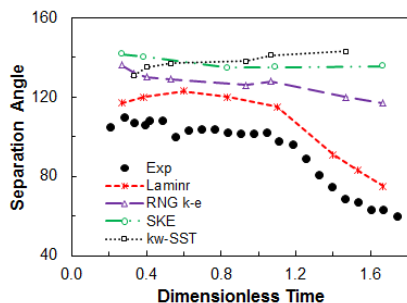


Figure 5 Image processing steps for determining the separation angle point along the head. The pixel values in panel are greyscale values where 255 = white, and 0 = black

For the CFD simulation results, flow separation was calculated from a wall shear stress profile across the head surface by extracting a line on the mid-plane line that intersected the manikin head. The separation angle was determined by locating the position where the wall shear stress was zero. The comparison results for the different viscous model shows the laminar model providing a correct profile of the separation angle reduction as the manikin decelerated over time – although the separation angle predicted is approximately 10% larger than the experimental results. The three turbulence models tested all over-predicted the separation angle with delayed separation, and failed to show the reduction in separation angle after the velocity dropped to half of its peak velocity ($Re \approx 1000$). The boundary layer remained attached to the surface and delayed the separation caused by excessive diffusion through addition of the eddy viscosity, which is related to the turbulent kinetic energy.

Wake flow from moving manikin

The wake flow produced from a moving manikin through its deceleration until it stops is shown in Figure 6.

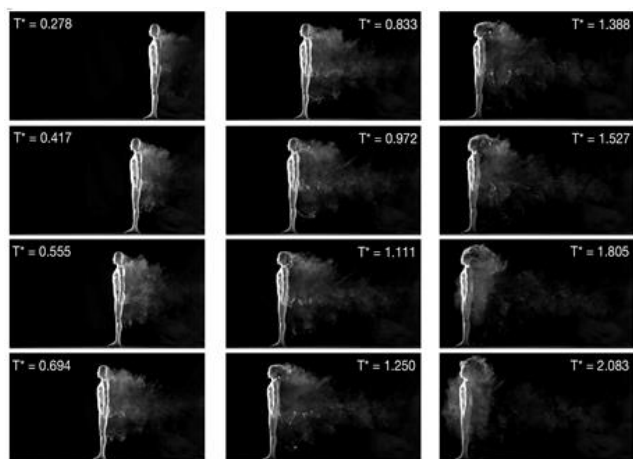


Figure 6 High speed photography showing the wake flow produced by the moving manikin starting at $T^*=0.278$ and shown at every $T^*=0.139$ (every 100 images) except for the last two images.

The wake initially starts small but develops as the flow becomes entrained in the region behind the manikin. There are clear flow separation points that characterise the wake, which are the separation at the head, and hand tip. Interestingly after the

manikin has come to a stop after $T^* = 1.667$ the wake flow catches up and passes the manikin. Exposure to contaminants in the breathing region is enhanced during this period.

Velocity contour and vectors were extracted from the CFD simulations and shown in Fig 7. At peak velocity ($T^* = 0.333$), the airflow was driven from the forehead towards the back of the head and shoulder, where a significant downwash (the change in direction of air deflected by the manikin) was observed in the wake region (Figure 4). At the lower part of the body, a jet protruded through the gap of legs and counteracted with the downwash flow thus generating a downward flow towards the ground and circulated in an anti-clockwise direction behind the lower legs. During the deceleration process ($T^* = 1.000$), flow at the back was weakened, and the smoke visualization at the same time also observed a diluted region close to the back. Under decreased velocities the downwash at the back region became weak and an upward trend started to grow. The protruding jet towards the back of legs also decayed thus dissipated with the forward flow from the rear, resulting in a rapid reduction in the velocity in this area. An increase in the anti-clockwise recirculation region behind the lower legs was also found.

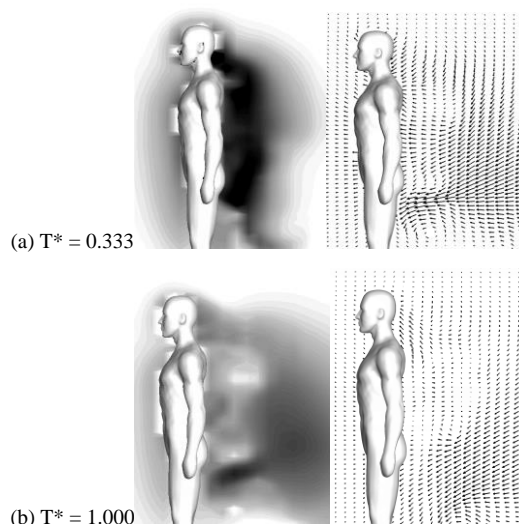


Figure 7 comparison of velocity magnitude contour and smoke visualization at peak velocity ($T=0.333$), deceleration ($T=1.000$) on the vertical middle plane

Particle re-suspension

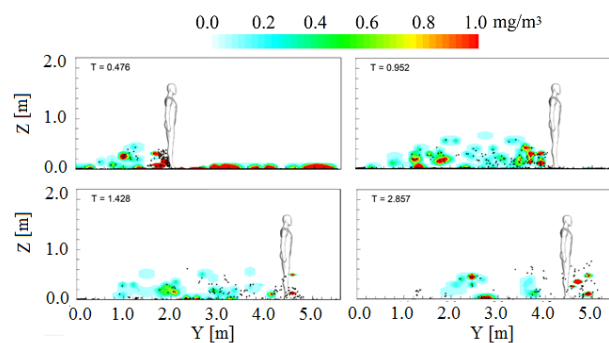


Figure 8 Particle concentration on the vertical middle plane and particle trajectory in the 3D room projected onto the vertical middle plane at different dimensionless time (motion ceased at $T^* = 0.952$)

The particle dispersion induced by human motion was simulated with a velocity of 0.2m/s –although this is low, we selected this velocity for Reynolds number matching with the experimental setup. The mass concentration on the vertical mid-plane and the

suspended particle trajectory in the 3D room projected onto the plane are shown in Fig 8.

Discussion

We presented a new smoke visualisation technique to allow different opportunities of visualising the human induced wake flow. Specifically we were able to capture the wake flow grow into a large plume and then when the manikin stopped moving, the wake continued its momentum and moved passed the manikin body. While the technique provides new visualisation, there are some limitations. The short distance travelled by the manikin was one limitation and this was constrained by the test chamber dimensions. This produced a very short transient velocity profile. Therefore we conclude that it is ideal for visualising and characterising the trailing wake and its movement passing over the manikin and into the breathing region – a physical behaviour that is difficult to replicate with traditional smoke visualisation in wind tunnels. To obtain steady flow velocity behaviour, the chamber can be extended to much longer distances to allow the motor to accelerate, then achieve some steady state before deceleration. However, larger distances make it difficult to maintain photographic resolution at high speed, greater demands on lighting, and computational resources (e.g. data transfer rate). Therefore it should be emphasised that this technique is not a substitute for steady state flow analysis, and even so this would simply be replicating a wind tunnel exercise except that the air flow is moving in a different frame of reference.

The CFD simulations showed demonstrate the importance of using the correct viscous model to represent the physical fluid dynamic behaviour. In the setup the laminar flow model provided correct flow behaviour in terms of flow separation. Many turbulence models in CFD, and in particular the $k-\epsilon$ and $k-\omega$ models (classified as RANS models) are designed for fully turbulent flows. When the flow regime is laminar dominant, the use of a turbulence model increases the flow diffusivity artificially through the addition of the eddy viscosity term building on top of the molecular viscosity. The effect of this came through in the flow separation analysis where the turbulence models severely overpredicted the separation angle; although it does reproduce the characteristic turbulent flow behaviour flow over bluff bodies.

Conclusions

By saturating a chamber with acetic acid, smoke originating from a moving object can be produced by introducing a reacting chemical such as cyclo-hexamine. The generated smoke traced the moving object providing the opportunity to investigate the effects of moving objects. The results showed wake flow forming behind the manikin which continued to travel under its own momentum and pass the manikin that had stopped moving. The wake plume passing into the breathing region has opportunity to increase contaminant particle inhalation exposure. The CFD simulation results showed a recirculation region behind the head, an upward flow in front of the upper body and a downwash flow at the back where highest velocity in the flow field occurs. Particles originating from the floor lifted off the ground due to the flow entrainment. However, at the very low velocity the particle re-suspension was limited to the lower half of the body region. Future work needs to create an experimental technique that will allow the manikin to move at faster rates.

Acknowledgement

The authors gratefully acknowledge the financial support provided by the Australian Research Council (project ID: DP160101953)

References

- [1] Ge Q, Li X, Inthavong K, and Tu J, Numerical study of the effects of human body heat on particle transport and inhalation in indoor environment. *Building and Environment* 2013; 59(0): 1-9.
- [2] Inthavong K, Mouritz AP, Dong J, and Tu JY, Inhalation and deposition of carbon and glass composite fibre in the respiratory airway. *Journal of Aerosol Science* 2013; 65: 58-68.
- [3] Kennedy NJ and Hinds WC, Inhalability of large solid particles. *Journal of Aerosol Science* 2002; 33: 237-255.
- [4] Li X, Inthavong K, and Tu J, Numerical investigation of micron particle inhalation by standing thermal manikins in horizontal airflows. *Indoor and Built Environment* 2014.
- [5] Brohus H, Balling KD, and Jeppesen D, Influence of movements on contaminant transport in an operating room. *Indoor Air* 2006; 16(5): 356-372.
- [6] Hang J, Li Y, and Jin R, The influence of human walking on the flow and airborne transmission in a six-bed isolation room: Tracer gas simulation. *Building and Environment* 2014; 77(0): 119-134.
- [7] Oberoi RC, Choi J-I, Edwards JR, Rosati JA, Thornburg J, and Rodes CE, Human-Induced Particle Re-Suspension in a Room. *Aerosol Science and Technology* 2010; 44(3): 216-229.
- [8] Wang J and Chow T-T, Numerical investigation of influence of human walking on dispersion and deposition of expiratory droplets in airborne infection isolation room. *Building and Environment* 2011; 46(10): 1993-2002.
- [9] Choi JI and Edwards JR, Large-eddy simulation of human-induced contaminant transport in room compartments. *Indoor Air* 2012; 22(1): 77-87.
- [10] Qian J and Ferro AR, Resuspension of Dust Particles in a Chamber and Associated Environmental Factors. *Aerosol Science and Technology* 2008; 42(7): 566-578.
- [11] You S and Wan MP, Experimental investigation and modelling of human-walking-induced particle resuspension. *Indoor and Built Environment* 2015; 24(4): 564-576.
- [12] Gomes C, Freihaut J, and Bahnfleth W, Resuspension of allergen-containing particles under mechanical and aerodynamic disturbances from human walking. *Atmospheric Environment* 2007; 41(25): 5257-5270.
- [13] George DK, Flynn MR, and Goodman R, The Impact of Boundary Layer Separation on Local Exhaust Design and Worker Exposure. *Applied Occupational and Environmental Hygiene* 1990; 5(8): 501-509.
- [14] Kulmala I, Saamanen A, and Enbom S, The effect of contaminant source location on worker exposure in the near-wake region. *Ann Occup Hyg* 1996; 40(5): 511-23.
- [15] Leder A and Grebin U, Flow-visualizations behind a high diver. *Journal of Visualization* 2003; 6(4): 328-328.
- [16] Sohankar A, Mohagheghian S, Dehghan AA, and Dehghan Manshadi M, A smoke visualization study of the flow over a square cylinder at incidence and tandem square cylinders. *Journal of Visualization* 2015: 1-17..